Published in final edited form as:
Cell Metab. 2009 November ; 10(5): 366–378. doi:10.1016/j.cmet.2009.09.010.

KSR2 Is An Essential Regulator of AMP Kinase, Energy Expenditure, and Insulin Sensitivity

Diane L. Costanzo-Garvey[1], **Paul T. Pfluger**[2], **Michele K. Dougherty**[3], **Jeffery L. Stock**[4], **Matthew Boehm**[1], **Oleg Chaika**[1], **Mario R. Fernandez**[1], **Kurt Fisher**[1], **Robert L. Kortum**[1], **Eun-Gyoung Hong**[5], **John Y. Jun**[5], **Hwi Jin Ko**[5,*], **Aimee Schreiner**[1], **Deanna J. Volle**[1], **Tina Treece**[1], **Amy L Swift**[6], **Mike Winer**[6], **Denise Chen**[6], **Min Wu**[6], **Lisa R. Leon**[7], **Andrey S. Shaw**[8], **John McNeish**[4,¶], **Jason K. Kim**[5,*], **Deborah K. Morrison**[3], **Matthias H. Tschöp**[2], and **Robert E. Lewis**[1,§]

[1]Eppley Institute for Research in Cancer and Allied Diseases, University of Nebraska Medical Center, Omaha, NE 68198-7696

[2]Obesity Research Center, Department of Medicine, University of Cincinnati, Cincinnati, OH, USA

[3]Laboratory of Cell and Developmental Signaling, Center for Cancer Research, NCI-Frederick, National Institutes of Health, Frederick, Maryland 21702, USA

[4]Genetic Technologies, Pfizer Global Research and Development, Groton 06340, Connecticut, USA

[5]Department of Cellular & Molecular Physiology, Penn State Mouse Metabolic Phenotyping Center, Pennsylvania State College of Medicine, Hershey, PA 17033, USA

[6]Seahorse Bioscience, 16 Esquire Road, North Billerica, MA 01862, USA

[7]Thermal Mountain Medicine Division, US Army Research Institute Environmental Medicine, Natick, MA 01760-5007

[8]Howard Hughes Medical Institute, and Department of Pathology and Immunology, Washington University School of Medicine, St. Louis, Missouri 63110, USA

Summary

Kinase Suppressors of Ras 1 and 2 (KSR1 and KSR2) function as molecular scaffolds to potently regulate the MAP kinases ERK1/2 and affect multiple cell fates. Here we show that KSR2 interacts with and modulates the activity of AMPK. KSR2 regulates AMPK-dependent glucose uptake and fatty acid oxidation in mouse embryo fibroblasts and glycolysis in a neuronal cell line. Disruption of KSR2 *in vivo* impairs AMPK-regulated processes affecting fatty acid oxidation and thermogenesis to cause obesity. Despite their increased adiposity, *ksr2*$^{-/-}$ mice are hypophagic and hyperactive, but expend less energy than wild type mice. In addition, hyperinsulinemic-euglycemic clamp studies reveal that *ksr2*$^{-/-}$ mice are profoundly insulin resistant. The expression of genes mediating oxidative phosphorylation is also down regulated in the adipose tissue of *ksr2*$^{-/-}$ mice. These data demonstrate

§correspondence: rlewis@unmc.edu
*current address: Program in Molecular Medicine, University of Massachusetts Medical School, 373 Plantation Street, Worcester, MA 01605, USA
¶current address: Pfizer Regenerative Medicine, Cambridge, MA 02139, USA

that *ksr2*$^{-/-}$ mice are highly efficient in conserving energy, revealing a novel role for KSR2 in AMPK-mediated regulation of energy metabolism.

Introduction

Molecular scaffolds, which coordinate the interaction of signaling molecules to affect efficient signal transduction (Burack and Shaw, 2000; Morrison and Davis, 2003), have the potential to serve as organizing nodes for multiple biological inputs. Kinase Suppressor of Ras 1 (KSR1) (Kortum and Lewis, 2004; Nguyen et al., 2002) serves as a scaffold for the coordination of signals through the Raf/MEK/ERK kinase cascade. Manipulation of KSR1 reveals its role in regulating the transforming potential of oncogenic Ras, neuronal and adipocyte differentiation, and replicative life span (Kortum et al., 2005; Kortum et al., 2006; Kortum and Lewis, 2004; Muller et al., 2000). A related protein, KSR2, has been detected in *C. elegans*, and humans (Channavajhala et al., 2003; Ohmachi et al., 2002). In *C. elegans*, KSR2 is required for germline meiotic progression and functions redundantly with KSR1 in excretion, vulva development, and spicule formation. Thus, KSR proteins appear to play critical roles in regulating multiple cell fates.

Cells must sense the nutritional status of the extracellular environment, monitor intracellular energy stores and integrate that information with intracellular pathways that drive cell fate. The trimeric AMP-activated protein kinase (AMPK) is a critical regulator of energy homeostasis that is activated when the nutritional environment is poor and intracellular ATP levels are low (Hardie, 2007). Under conditions of energy stress, ATP levels fall, and levels of the allosteric activator AMP rise, which promotes binding of the catalytic AMPK α-subunit to the γ-subunit, and protects against de-phosphorylation of a critical threonine in the activation loop of the α-subunit kinase domain (Sanders et al., 2007). ATP antagonizes the action of AMP on AMPK, making AMPK a sensor of cellular energy stores.

Upon activation, AMPK stimulates metabolic enzymes and induces gene expression programs to promote catabolic activity and inhibit anabolic activity. AMPK stimulates insulin-independent glucose uptake in muscle in response to exercise and hypoxia (Mu et al., 2001), and promotes the β-oxidation of long-chain fatty acids by phosphorylating and inhibiting acetyl-CoA carboxylase (ACC), the rate-limiting enzyme of malonyl-CoA synthesis (Ruderman et al., 2003). Malonyl-CoA is both a key substrate for fatty acid synthesis and an inhibitor of carnitine palmitoyltransferase 1 (CPT1), which mediates import of fatty acyl-CoA molecules into the mitochondria for oxidation. By inhibiting ACC, AMPK inhibits the synthesis of fatty acids and promotes their metabolism to generate ATP.

The mechanisms linking dietary nutrients and AMP-regulated energy metabolism to cell fate are incompletely understood. Our analysis of the scaffold KSR2, however, provides a missing link. Here we show that KSR2 interacts with AMPK in a functionally relevant manner *in vitro* and *in vivo*. In cultured cells AMPK-dependent effects on basal glucose uptake, fatty acid oxidation and glycolysis are enhanced by KSR2. Gene disruption of *ksr2* reduces the glucose lowering capacity of an AMPK agonist *in vivo*. The white adipose tissue of *ksr2*$^{-/-}$ mice demonstrates defective phosphorylation of the AMPK substrate acetyl-CoA carboxylase, a key regulator of fatty acid synthesis and oxidation, and a down regulation of genes involved in oxidative phosphorylation. As a consequence of these impaired AMPK-dependent mechanisms, *ksr2*$^{-/-}$ mice are obese and insulin resistant. In contrast to most other animal models of obesity, *ksr2*$^{-/-}$ mice are hypophagic and more active. However, they expend less energy than wild type mice. These data reveal a novel role for KSR2 as a critical regulator of cellular energy balance affecting lipid and glucose metabolism.

Results

KSR1 and KSR2 interact with AMPK

We used mass spectrometry to identify novel regulators that may affect KSR1 and KSR2 function. Previously reported KSR1-interacting molecules (Muller et al., 2001; Ory et al., 2003; Ritt et al., 2007), including HSP90, HSP70, Cdc37, C-Tak1 and PP2A were detected in association with KSR2 as were peptidergic components of the α1, α2, β1 and γ1 subunits of AMP-activated protein kinase (AMPK) (Figure 1A). This interaction was verified by the co-precipitation of endogenous AMPK α1 subunit in immunoprecipitates of KSR2 but not in immunoprecipitates of KSR1 (Figure 1B). When both AMPKα and KSR1 were overexpressed, an interaction between the two proteins could be detected. However, when compared for their relative ability to precipitate endogenous or ectopic AMPKα, KSR2 consistently precipitated more AMPK than did KSR1 (Figure 1C). To determine the sites required for interaction with AMPK, full length and truncated versions of KSR1 and KSR2 were expressed in 293T or COS-7 cells and their ability to precipitate endogenous AMPK or the ectopic AMPKα subunit was tested. Deletion analysis indicated that the CA3 region contributes to the interaction of the AMPKα subunit with KSR1 (Figure 1D and E) and that the CA3 region and amino acids unique to KSR2 intervening between the CA2 and CA3 region (Dougherty et al., 2009) each contributed to the ability of KSR2 to interact with the AMPKα subunit (Figure 1F-G). The observation that KSR2 retains additional sequences contributing to its interaction with AMPK may explain its ability to precipitate a proportionally greater amount of AMPK.

KSR2 promotes glucose and fatty acid metabolism

We tested whether mutations that impaired the interaction of AMPK with KSR1 or KSR2 affected ERK activation. The ΔCA3 mutation severely affected maximal activation of ERK by KSR proteins as observed previously for KSR1 (Michaud et al., 1997) (Figures 2A and S2A). However, KSR2Δ327-392 effects on ERK activation were equivalent to KSR2 (Figure 2A). These data indicate it is unlikely ERK activation plays a role in mediating the effects of KSR2 on AMPK signaling.

AMPK stimulates glucose uptake and the oxidation of fatty acids by mitochondria, thereby promoting ATP synthesis (Ruderman et al., 2003). To test whether KSR proteins affect these catabolic functions of AMPK, we generated *ksr2*$^{-/-}$ mice (Figure S1) and *ksr2*$^{-/-}$ MEFs. We measured glucose uptake in *ksr2*$^{-/-}$ and *ksr1*$^{-/-}$ mouse embryo fibroblasts (MEFs) and in null MEFs expressing their respective cognate *ksr* transgenes. Though MEFs do not express detectable KSR2 (not shown), expression of ectopic KSR2 in *ksr2*$^{-/-}$ MEFs increased basal glucose uptake 5-fold (Figure 2B) and expression of KSR1 in *ksr1*$^{-/-}$ MEFs increased basal glucose uptake 2-fold (Figure S2B). Deletion of the CA3 region (KSR2.ΔCA3) modestly impaired basal glucose uptake, but deletion of sequences between the CA2 and the CA3 regions (KSR2.Δ327-392) decreased KSR2-induced glucose uptake by 50% (Figure 2B). Deletion of the CA3 region (KSR1.ΔCA3) was sufficient to significantly disrupt the effects of KSR1 on basal glucose uptake (Figure S2B).

We then tested whether KSR2 or KSR1 affected cellular fatty acid metabolism. The rate of oxygen consumption (OCR) was used as an index of oxidative phosphorylation (Wu et al., 2007). OCR in *ksr2*$^{-/-}$ or *ksr1*$^{-/-}$ MEFs was compared to OCR in *ksr2*$^{-/-}$ or *ksr1*$^{-/-}$ MEFs expressing full length KSR2 or KSR1, respectively. In both *ksr2*$^{-/-}$ and *ksr1*$^{-/-}$ MEFs, palmitate had little or no ability to stimulate oxygen consumption. However, the reintroduction of KSR2 (Figure 2C) or KSR1 (Figure S2C) restored oxidation of palmitate. As with glucose uptake, disrupting the interaction of KSR2 or KSR1 with AMPK prevented restoration of fatty acid oxidation (Figures 2C and S2C).

The neuroblastoma X glioma hybrid cell line NG108-15 expresses endogenous KSR2 (Dougherty et al., 2009). An shRNA was constructed to knock down KSR2 expression in these cells. In culture, neuronal cell lines in general, and NG108-15 cells in particular, synthesize ATP primarily from glycolysis (Ray et al., 1991). Since AMPK activation promotes glycolysis (Marsin et al., 2000), we examined the ability of KSR2 knockdown with and without the co-expression of a constitutively active AMPK construct to regulate glycolysis in NG108-15 cells. As an index of lactate production, extracellular acidification was markedly reduced in these cells when RNAi was used to inhibit KSR2 expression. However, expression of a constitutively active AMPK (Stein et al., 2000) restored glycolysis to levels seen in control cells (Figure 2D).

Phosphorylation of Thr172 on the effector loop of AMPK promotes its activity (Stein et al., 2000). In MEFs the presence or absence of KSR2 did not affect AMPK Thr172 phosphorylation (not shown), suggesting that AMPK signaling may require KSR2 for proper spatial regulation similar to its effect on ERK (Dougherty et al., 2009). However, in NG108-15 cells, loss of KSR2 inhibits the phosphorylation of AMPK on Thr172 in response to AICAR and modestly impairs phosphorylation of the AMPK substrate ACC (Figure 2E). These data support the conclusion that KSR2 is an AMPK regulator. To determine the relative impact of KSR1 and KSR2 on AMPK function and fatty acid metabolism *in vivo* we examined the metabolic phenotype of *ksr1*$^{-/-}$ and *ksr2*$^{-/-}$ mice.

Loss of *ksr2* causes obesity

KSR2 protein is detectable by western blot only in brain (Figure S1C). Therefore, we determined the relative abundance of *ksr2* mRNA in various tissues (Figure 3A). Consistent with western blot analysis, *ksr2* mRNA is approximately 100-fold more abundant in brain than in skeletal muscle or liver. *ksr2* mRNA is detectable at low levels in adipose tissue. In contrast, *ksr1* mRNA is expressed strongly in skeletal muscle but present at approximately one third that level in brain and 5% of that level in adipose tissue. *ksr1*$^{-/-}$ mice have been previously reported to have enlarged adipocytes but normal amounts of all adipose tissues (Kortum et al., 2005). Further analysis revealed no altered response to an AMPK agonist (Figure S3) and no overt metabolic defects (Figure S4 and Table S1) in *ksr1*$^{-/-}$ mice.

To test the role of KSR2 in the regulation of AMPK-mediated signaling, we targeted exon 4 within the *ksr2* locus for deletion in mice (Figure S1). The *ksr2*-null allele was transmitted through the germ line, and heterozygous intercrosses yielded all three genotypes in a ratio close to the expected Mendelian distribution (relative ratios *ksr2*$^{+/+}$ 1, *ksr2*$^{+/-}$ 2.25, *ksr2*$^{-/-}$ 0.91; n = 441). During development *in utero* and at birth *ksr2*$^{-/-}$ mice were identical in size and weight to wild type and *ksr2*$^{+/-}$ mice (Figure 3B, left panel). However, while nursing, *ksr2*$^{-/-}$ mice grew at approximately 50% the rate observed in wild type and *ksr2*$^{+/-}$ mice (Figure 3B, center panel). Thirty two percent of *ksr2*$^{-/-}$ mice (31 of 98) failed to survive until weaning. Premature death was not due to the failure of *ksr2*$^{-/-}$ pups to nurse properly as all mice had milk in their stomachs upon necropsy. The addition of foster mothers did not improve survival. Furthermore, nutrient absorption was identical in wild type and *ksr2*$^{-/-}$ mice (not shown). We measured the growth rate of surviving *ksr2*$^{-/-}$ mice and observed that the *ksr2*$^{-/-}$ mice attained body weights similar to wild type and *ksr2*$^{+/-}$ mice 6-10 weeks after birth (Figure 3C). At 20-24 weeks of age, *ksr2*$^{-/-}$ mice exceeded the body weight of their wild type and *ksr2*$^{+/-}$ littermates and became obese (Figure 3B, right panel). Interestingly, disruption of *ksr2*$^{-/-}$ caused a doubling in fat mass and a 15% decrease in lean mass even before body weight differences became apparent (Figure 3D). All adipose depots from *ksr2*$^{-/-}$ mice were significantly increased in mass relative to wild type mice (Figure 3E). Histological analysis demonstrated that the cross-sectional area of adipocytes from white adipose tissue in *ksr2*$^{-/-}$ mice was increased in size relative to wild type mice (Figure 3F).

ksr2 promotes AMPK signaling *in vivo*

We tested whether an interaction between endogenous KSR2 and AMPK could be detected similar to that observed when KSR2 was overexpressed in COS7 cells (Figure 1). Brain lysates from wild type and *ksr2*$^{-/-}$ mice were precipitated with antibodies against the AMPKα subunit and probed for KSR2 on western blot. KSR2 was detected in anti-AMPKα immunoprecipitates from WT brain but not detected in anti-AMPKα immunoprecipitates from *ksr2*$^{-/-}$ brain or from wild type brain immunoprecipitated with a non-immune antibody (Figure 3G).

To determine whether *ksr2*$^{-/-}$ mice have defects in AMPK signaling, we tested the ability of an intraperitoneal injection of the AMPK agonist AICAR to lower blood glucose. Wild type mice showed a rapid and sustained reduction in blood glucose in response to the AMPK agonist AICAR that was not altered by deletion of *ksr1* (Figure S3). However, disruption of *ksr2* in mice delayed the onset of the drop in blood glucose and reduced the extent of the decrease (Figure 3H). Given the effect of AICAR in *ksr2*$^{-/-}$ mice, the phosphorylation state of AMPK and ACC was examined in white adipose tissue. While wild type mice showed strong phosphorylation of AMPK and ACC following AICAR injection, disruption of *ksr2* impaired their phosphorylation in white adipose tissue (Figure 3I). Furthermore, when explants of subcutaneous adipose tissue were isolated and incubated *ex vivo* with AICAR, wild type adipose tissue showed robust phosphorylation of AMPK on Thr172 and of ACC on Ser79. However, AMPK and ACC from *ksr2*$^{-/-}$ adipose tissue remained unphosphorylated and ACC expression was markedly reduced (Figure 3J). These data suggest that, despite its low level of expression (Figure 3A), KSR2 functions in a cell autonomous manner in adipose tissue.

KSR2 controls energy expenditure

We next tested the hypothesis that due to the role of KSR2 in controlling AMPK function, global *ksr2* gene disruption would result in impaired energy metabolism. Large lipid vesicles were detected in the brown adipose tissue (BAT) of *ksr2*$^{-/-}$ mice that were absent in wild type mice (Figure 4A). BAT is the major site of adaptive thermogenesis in rodents and adaptive thermogenesis protects mammals during cold exposure and regulates energy balance to compensate for alterations in nutrient intake (Lowell and Spiegelman, 2000). We next assessed whether this lipid accumulation was reflected in reduced heat generation. The rectal temperature of wild type and *ksr2*$^{-/-}$ mice was compared during distinct diurnal periods. Deletion of KSR2 lowered rectal temperature by as much as 1.5°C (Figure 4B) and modestly decreased UCP1 mRNA expression (Figure 4C, left panel) and protein levels (Figure 4C, right panel).

Hyperphagia is considered a hallmark of numerous well-characterized rodent models of obesity (Bray and York, 1979). However, obese *ksr2*$^{-/-}$ mice actually consumed less food than wild type mice in spite of increased adiposity (Figure 4D). Consistent with the observed increase in fat mass, serum leptin levels in the *ksr2*$^{-/-}$ mice were elevated seven-fold in females and 12-fold in males (Figure 4E). The morbid obesity and hyperleptinemia suggested massive leptin resistance. However, injection of leptin suppressed food consumption to the same degree in both wild type and *ksr2*$^{-/-}$ mice (Figure 4F). Key orexigenic hypothalamic neuropeptides agouti-related peptide (AgRP) and neuropeptide Y (NPY) (Ollmann et al., 1997; Schwartz et al., 1996), and anorexigenic neuropeptides proopiomelanocortin (POMC) and cocaine- and amphetamine-regulated transcript (CART) (Kristensen et al., 1998) were unchanged in *ksr2*$^{-/-}$ mice suggesting a novel compensatory mechanism independent from known major pathways of adipocyte-hypothalamus communication (Figure 4G).

Consistent with the ability of KSR2 to alter the rate of oxygen consumption *in vitro* (Figure 2D), young male *ksr2*$^{-/-}$ mice in total consume less oxygen than wild type mice and produce less CO_2 (Figure 5A). In females, a similar trend is observable. These data support the

conclusion that oxidative phosphorylation is impaired by the disruption of *ksr2*. Respiratory quotient (RQ) is lower in *ksr2*$^{-/-}$ mice during the dark cycle relative to wild type mice (Figures 5A and S5A), indicating a preference for fatty acids as metabolic substrate of choice or a relative resistance to carbohydrate metabolism during active periods. General, ambulatory and stationary motor activity is increased in *ksr2*$^{-/-}$ mice (Figure 5B and S5B-D), despite their obesity. The consequence of such energy balance physiology responses to the disruption of *ksr2* would result in a decreased amount of energy stored as fat. However, overall *ksr2*$^{-/-}$ mice expend substantially less energy (Figures 5C) and therefore accrue larger fat deposits than wild type mice. In order to exclude a potential artifact resulting from relative cold-exposure of *ksr2*$^{-/-}$ and wild type mice while being studied at room temperature, we re-analyzed their metabolic phenotype at thermoneutrality (32°C). *ksr2*$^{-/-}$ mice exhibited significantly lower oxygen consumption under those conditions (Fig. 5D), consistent with an ambient temperature-independent and physiologically relevant deficit in basal metabolic rate. Thus, despite compensatory feeding and nutrient partitioning responses to their increased adiposity, *ksr2*$^{-/-}$ mice become obese due to low resting thermogenesis and high energy efficiency.

ksr2$^{-/-}$ mice are insulin resistant

Obesity is associated with elevated serum lipids and predisposes rodents and humans to impaired glucose homeostasis (Lazar, 2005). We find that the absence of KSR2 replicates both conditions since *ksr2*$^{-/-}$ mice show elevated lipolysis, free fatty acids, triglycerides (Figure 6A) and fasting insulin levels (Figure 6B). Adiponectin, resistin, PAI-1, IGF-1, and thyroxin were not significantly altered by disruption of *ksr2*. MCP-1 was significantly elevated in male but not female *ksr2*$^{-/-}$ mice (Figure S6). These data suggested that elevated endogenous insulin levels might be compensating for peripheral insulin resistance caused by the disruption of *ksr2*. We, therefore, performed hyperinsulinemic euglycemic clamps on wild type, *ksr1*$^{-/-}$, and obese *ksr2*$^{-/-}$ mice. Glucose homeostasis in *ksr1*$^{-/-}$ mice mirrored that of wild type mice (Table S1). In contrast, *ksr2*$^{-/-}$ mice maintained comparable blood glucose concentrations only at glucose infusion rates that ranged between 20-50% of that observed in wild type mice (Figure 6C). Though hepatic glucose production (HGP) was reduced in *ksr2*$^{-/-}$ mice in comparison to wild type mice, the ability of insulin to suppress HGP in the null mice was markedly suppressed (Figure 6D). Similarly, whole body glucose turnover, glycolysis and glycogen production were reduced in knockout mice (Figure 6E). These data are consistent with markedly reduced glycogen content in the livers and glycolytic muscle of *ksr2*$^{-/-}$ mice (Figure 6F). To estimate insulin-stimulated glucose uptake in individual tissues, 2-deoxy-D-[1-^{14}C] glucose was administered as a bolus (10 mCi) 75 min after the start of clamp. In comparison to wild type mice, *ksr2*$^{-/-}$ mice showed profound insulin resistance in skeletal muscle (gastrocnemius) and both white (epididymal) and brown adipose tissue (Figure 6G). In combination with the effect on HGP, these data reveal that disruption of *ksr2* impairs glucose uptake at the major sites of insulin action.

To test whether the effect of KSR2 disruption had a cell autonomous effect on insulin-stimulated glucose uptake, we examined glucose uptake in isolated EDL muscles from wild type and *ksr2*$^{-/-}$ mice. Insulin significantly stimulated glucose uptake in the isolated muscle from either genotype to a similar degree (Figure 6H). In contrast, the AMPK agonist AICAR had a small but significant impact on glucose uptake in wild type EDL muscle but no effect on EDL muscle from *ksr2*$^{-/-}$ mice. These data suggest that KSR2 has a direct effect on AMPK-stimulated glucose uptake in EDL muscle. However, the insulin resistance observed in skeletal muscle of *ksr2*$^{-/-}$ mice appears to be a non-cell autonomous effect, perhaps secondary to the obesity and impaired lipid metabolism caused by KSR2 disruption (Bergman et al., 2006).

KSR2 coordinates OXPHOS gene expression

The observation that KSR2 expression regulated oxidative metabolism *in vitro* (Figure 2C), led us to examine gene expression in the white adipose tissue of *ksr2*$^{-/-}$ and wild type mice. Gene Set Enrichment Analysis (GSEA) (Subramanian et al., 2005) revealed that gene sets previously identified as down regulated in obese mouse models and in some humans with abnormal glucose tolerance are regulated by *ksr2* (Figure S7A, Supplemental Table S2). Strongest among these was a gene set previously shown to be down regulated in *ob/ob* mice (Nadler et al., 2000). A notable number of sets that included genes for oxidative metabolism were also down regulated in *ksr2*$^{-/-}$ mice. A subset of oxidative phosphorylation genes co-regulated across different mouse tissues (OXPHOS-CR) was identified previously (Mootha et al., 2003). This gene set corresponds to two thirds of the genes encoding the oxidative phosphorylation biochemical pathway. The OXPHOS-CR gene set is reported to be down regulated in skeletal muscle of some humans with impaired glucose tolerance and correlated with changes in total body metabolism. We examined the expression of a custom gene set corresponding to the mouse orthologs (mOXPHOS-CR) and determined that this set was significantly down regulated ($p<.001$, NES = -2.39, FDR<.001) in the white adipose tissue of *ksr2*$^{-/-}$ mice. 83% (20 of 24) of the genes demonstrated lower expression in *ksr2*$^{-/-}$ mice in comparison to wild type mice (Figure S7). The transcriptional co-regulator PGC1α is a potent regulator of OXPHOS-CR genes (Mootha et al., 2003). Microarray analysis revealed that PGC1α is also markedly decreased in the white adipose tissue of *ksr2*$^{-/-}$ mice (Figure S7). These data demonstrate that the AMPK regulator KSR2 plays a potent role in controlling the expression of PGC1α-dependent gene programs whose alteration may contribute to impaired glucose tolerance in KSR2$^{-/-}$ mice.

Discussion

In this study, we show that the molecular scaffold KSR2 is an essential regulator of AMPK activity controlling cellular thermogenesis, fat oxidation, and glucose metabolism. These data suggest a model (Figure 7) whereby a decrease in AMPK function impairs fatty acid oxidation and increases lipid storage, contributing to obesity and insulin resistance in *ksr2*$^{-/-}$ mice. In wild type mice, KSR2 interacts with AMPK to negatively regulate ACC and promote the expression of PGC1α-dependent OXPHOS genes. Inhibition of ACC prevents the synthesis of the CPT1 allosteric negative regulator malonyl CoA. Together with OXPHOS gene expression, elevated CPT1 activity enhances the oxidation of fatty acids and reduces their storage as triglycerides (TG). In the absence of KSR2 AMPK function is impaired, OXPHOS gene expression declines, ACC activity is deregulated causing decreased long chain fatty acid uptake into mitochondria via CPT1 and enhanced triglyceride synthesis, which promotes obesity. These findings reveal a novel pathway regulating energy expenditure and glucose metabolism, the elucidation of which may facilitate therapeutic intervention in obesity.

It remains unclear to what extent specific tissues contribute to the metabolic defects caused by KSR2 disruption. *Ex vivo* experiments suggest a role for KSR2 in adipose tissue and muscle. However, KSR2 is detectable by western blot only in the brain, and mRNA profiling detects much lower levels of KSR2 in muscle, liver, and adipose tissue. These data suggest that important actions of KSR2 on AMPK are probably exerted within the central nervous system.

Resting metabolic rate is the major contributor to obligatory energy expenditure and is strongly associated with fat-free mass (Cunningham, 1991). However, fat-free mass accounts for only 70% to 80% of the variability in resting metabolic rate (Sparti et al., 1997). Genetically determined differences in the ability of organisms to consume oxygen to make ATP have been proposed as an explanation for at least some of the remaining variability (Harper et al., 2008). The reduced oxygen consumption and energy efficiency of *ksr2*$^{-/-}$ mice identify *ksr2* as a novel genetic determinant of metabolic rate. To some extent, decreased energy expenditure

in *ksr2*$^{-/-}$ mice could be ascribed to the decrease in UCP1 expression, which might contribute to the 1.5°C drop in rectal temperature of *ksr2*$^{-/-}$ mice. The reduced rectal temperature of *ksr2*$^{-/-}$ mice therefore suggests that *ksr2* is essential for the physiological regulation of resting thermogenesis.

Through its phosphorylation of ACC, AMPK plays a critical role in determining whether fatty acids are oxidized in mitochondria to generate ATP or stored as triglycerides. Our *in vivo* and *ex vivo* data demonstrate that deletion of KSR2 in white adipose tissue impairs the ability of AMPK to phosphorylate ACC, which should inhibit fatty acid oxidation and promote triglyceride storage (Ruderman et al., 2003). This defect provides a simple explanation for the increased fat mass of *ksr2*$^{-/-}$ mice (Brommage et al., 2008). Accordingly, *ampkα2*$^{-/-}$ mice share traits with *ksr2*$^{-/-}$ mice. On a high fat diet, *ampkα2*$^{-/-}$ mice demonstrate elevated body weight, morbidly increased adipose mass and adipocyte hypertrophy without an increase in food intake relative to control mice (Villena et al., 2004). Similar to *ksr2*$^{-/-}$ mice, deletion of the AMPK α2 subunit causes insulin resistance and AICAR intolerance (Viollet et al., 2003). Also consistent with our findings, loss of AMPK signaling that results from hepatic disruption of the AMPK-kinase, LKB1, causes hyperglycemia and glucose intolerance, while not impairing insulin action (Shaw et al., 2005). Thus, KSR2 may affect cell autonomous energy homeostasis in multiple tissues by directly modulating lipid and glucose metabolism via AMPK, while behavioral phenotypes of KSR-deficient mice such as hypophagia and hyperactivity are likely compensatory responses for body setpoint defense.

We performed microarray analysis on mRNA isolated from wild type and *ksr2*$^{-/-}$ adipose tissue to identify genetic pathways affected by the deletion of KSR2. GSEA of microarray data identified curated gene sets that are significantly regulated by the presence or absence of KSR2 (Figure S7 and Table S2). Grouping the highest ranking ($p = 0.000$; FDR ≤ 0.001; FWER ≤ 0.045) gene sets according to overlapping genes identifies three general cellular functions regulated by KSR2. In white adipose tissue, KSR2 appears to most potently affect genes regulating adipocyte differentiation, genes involved in oxidative phosphorylation, and genes affecting the metabolism of branched-chain amino acids and short chain lipids. KSR2-dependent regulation of genes controlling adipocyte differentiation (e.g., Nadler Obesity Down, IDX TSA Up Cluster 6, and TNFα Down gene sets) plays a role in the increased adipocyte cell number observed in *ksr2*$^{-/-}$ mice. Decreased expression of genes involved in oxidative phosphorylation (e.g., Electron Transport, Mootha VoxPhos, and Mitochondria gene sets) likely contributes to the decreased ability of *ksr2*$^{-/-}$ mice to metabolize lipid and carbohydrate. Gene sets for branched chain amino acid catabolism, and propionate, butanoate and pyruvate metabolism represent key pathways that generate key substrates (e.g., acetyl-CoA, succinyl-CoA) to the TCA cycle and fatty acid synthesis. The regulation of these pathways by KSR2 suggests a role for the scaffold in controlling both the availability of these key substrates as well as the enzymes necessary for their metabolism. However, future experiments will be required to determine whether these changes in gene expression are mediated by the action of KSR2 in adipose tissue or in another tissue with prominent expression, like the brain.

KSR1 and KSR2 are best known for their function as scaffolds for the Raf/MEK/ERK signaling cassette, facilitating the activation of Raf and MEK (Dougherty et al., 2009; Kortum and Lewis, 2004; Nguyen et al., 2002). The interaction of AMPK with these molecular scaffolds raises the intriguing possibility that KSR proteins function not only as scaffolds, but also as components of an energy and nutrient sensor that couples information about the nutritional environment and intracellular energy status of a cell to a kinase cascade with potent effects on cell proliferation, differentiation, and survival. The discovery that C-TAK1/MARK3/Par1a, a member of the AMPK kinase family, phosphorylates KSR1 and inhibits its ability to promote the activation of MEK by Raf (Muller et al., 2001), supports this concept. In complex with

KSR2, AMPK might provide similar means to restrict energy-intensive proliferative stimuli emanating from activated ERK when ATP is limited. *ksr2*$^{-/-}$ mice might thus develop impaired metabolic homeostasis due to an inability to respond appropriately to energy deficits and curb ERK signaling when the nutritional environment is inadequate.

Consistent with that paradigm, our results demonstrate that disruption of *ksr2* causes obesity through a reduction in cellular energy consumption despite hypophagia. Therefore, our observations reveal *ksr2*$^{-/-}$ mice to be a novel model of obesity with potential relevance to obesity-related dysregulation of glucose metabolism. That molecular scaffolds regulating the activation of Raf, MEK, and ERK can have a profound effect on fat accumulation suggests that factors affecting energy balance may have previously unappreciated roles on MAP kinase signaling. In particular, future studies focusing on cell type-specific mechanisms of KSR2/AMPK interactions may provide important insight into novel mechanisms regulating physiological control of energy storage and expenditure with implications for glucose homeostasis.

Experimental Procedures

Mice

ksr1$^{-/-}$ mice were described previously (Kortum et al., 2005; Nguyen et al., 2002). Standard gene-targeting techniques and homologous recombination were used to generate *ksr2*$^{-/-}$ mutant mice. The Institutional Animal Care and Use Committee (University of Nebraska Medical Center, Omaha, NE) approved all studies. Animals were maintained on a 12-hour light/dark schedule (light on at 0600) and had free access to laboratory chow (Harlan Teklad LM 485) and water. All *in vivo* analyses were performed on mice of 3-7 months of age.

Cells

KSR1$^{-/-}$ and KSR2$^{-/-}$ MEFs were generated from day 13.5 embryos and immortalized by 3T9 protocol as described (Kortum and Lewis, 2004) or by expression of Sv40 Large T antigen. Expression of KSR1, KSR2 and corresponding mutants in MEFs was also measured as described previously (Kortum and Lewis, 2004). NG108-15 cells, COS-7 and 293T cells were obtained from ATCC.

Immunoprecipitation and Immunoblots

Immunoprecipitation were performed on post-nuclear membranes with antibodies to the FLAG, Pyo, and Myc epitope tags as described previously (Kortum and Lewis, 2004; Ritt et al., 2007). Antibodies for AMPKα, phospho-Thr172 AMPK, ACC, and phospho-Ser79 ACC, UCP1, and GAPDH were from Cell Signaling. Anti-KSR2 antibody 1G4 was from Abnova. Anti-α-tubulin antibodies were from Santa Cruz.

Glucose Uptake and ERK assays

Glucose uptake was measured with 2-deoxy-D[2,6-^{3}H]glucose in the presence or absence of 20 μM cytochalasin B and 200 μM phloretin as described previously (Chaika et al., 1999). ERK phosphorylation was quantified on the Odyssey system (LI-COR) with anti-phospho-ERK1/2 (Cell Signaling No. 9106) and anti-ERK1 (Santa Cruz Biotechnology, sc-93) primary antibodies and goat anti-mouse Alexa Fluor 680 (Invitrogen) and goat anti-rabbit IRDye 800 (Rockland) as secondary antibodies as described (Kortum and Lewis, 2004).

Fatty acid oxidation and glycolysis assays

Fatty acid oxidation (FAO) and glycolysis was determined by measuring oxygen consumption rate (OCR) and extracellular acidification rate, respectively, in cultured cells using the XF24 Analyzer (Seahorse Bioscience) (Wu et al., 2007).

KSR2 shRNA

A short hairpin targeting the nucleotides for amino acids 868-874 of mouse KSR2 was cloned into the lentiviral MISSION® pLKO.1-puro vector. Puromycin resistant cells were selected using 2 μg/ml puromycin (Sigma).

ksr1 and *ksr2* mRNA Quantification

Total RNA was isolated from selected mouse tissues using Tri-Reagent (Molecular Research Center, Inc). *ksr1*, *ksr2*, *GusB*, and *Tbp* were simultaneously quantified from 5 μg of total RNA using QuantiGene 2.0 Plex gene sets (Panomics), following the manufacturer's recommendations. Total RNA was hybridized to custom probe set 21121 for 24 hours at 54 ° C while shaking at 900 RPM with an orbital diameter of 3 mm before signal amplification and quantification using a Luminex 200 instrument. The median fluorescent intensity of at least 50 beads was used to determine the average gene expression for tissue samples from three mice performed in duplicate.

Quantitiative PCR

RNA was extracted from brown adipose tissue (BAT) and hypothalamus using TRizol reagent (Invitrogen), according to the manufacturers instructions. After subsequent DNase treatment, reverse transcriptions were performed using SuperScript III (Invitrogen) and Oligo-dT20 primers (Invitrogen). Real-time PCR for UCP1 in BAT and neuropeptides in hypothalamus, and the ribosomal house keeping gene L32, were performed on a Biorad iCycler using iQ SybrGreen Supermix (Biorad). Relative quantification of the target transcript in comparison to a reference transcript was calculated from the real-time PCR efficiencies and the crossing point deviation of the target sample versus its control (Pfaffl, 2001).

Body composition and adipocyte size

Body composition was measured using Nuclear Magnetic Resonance technology (NMR, EchoMRI, Quantitative Magnetic Resonance Body Composition Analyzer, Echo Medical Systems, LLC, Houston, TX, USA). Total adipose tissue from each depot was excised and the wet weight was determined. Abdominal, subcutaneous, and brown adipose tissue was fixed in Bouin's fixative, sectioned in a microtome and stained with hematoxylin and eosin. Adipocyte cross-sectional area was determined from photomicrographs of epididymal fat pads using IPLab software (Scanalytics Inc., Fairfax, VA)(Kortum et al., 2005).

In vivo metabolic phenotype analysis

Food intake was measured daily manually over five consecutive days in freely feeding mice. Total energy expenditure, locomotor activity, and respiratory quotient (relative rates of carbohydrate versus fat oxidation) of mice were determined by indirect calorimetry using a customized 32-cage indirect calorimetry system (TSE Systems Midland, MI). The mice were placed in the calorimetry system cages for up to 6 days and nights, with at least 24h for adaptation before data recording. For oxygen consumption measurements at thermoneutral conditions, the environmental temperature requiring the least energy for organismal heating or cooling processes was determined using indirect calorimetry within a climate control system. Thermoneutral zone for *ksr2*$^{-/-}$ and wild type mice was determined. Oxygen consumption

analysis was then performed to ascertain that the thermogenetic phenotype was not an artifact resulting from relative cold exposure of *ksr2*$^{-/-}$ and wild type mice.

Metabolite assays

Blood glucose was measured with an Ascensia Glucometer Elite (Fisher Scientific). Plasma insulin was measured with the Mouse Insulin Elisa Kit (ChrystalChem, Chicago, IL) using mouse standards. Serum free fatty acids were measured colorimetrically (Roche). Plasma triglycerides and glycerol were measured using the GPO-Trinder colorimetric assay kit (Sigma). Plasma leptin was measured using the Rat Leptin RIA kit (Linco Research, St Louis, MO). Glycogen content was analyzed with the Glucose HK assay (Sigma). For measurement of lipolysis, mice were fasted overnight for 12 h. Subcutaneous fat was excised, minced in Krebs-Ringers bicarbonate buffer at 37 °C for 3 h, and a sample of media was assayed for glycerol content using Free Glycerol Reagent (Sigma).

Ex vivo culture of white adipose tissue explants

Subcutaneous fat pads were removed from 7-month old wild type and *ksr2*$^{-/-}$ mice, prepared and treated as described (Gaidhu et al., 2009).

Ex vivo glucose uptake

Glucose uptake was measured in isolated EDL muscle from wild type and ksr2$^{-/-}$ mice using 2-deoxy-D[2,6-^{3}H]glucose and [^{14}C]mannitol as described previously (Sakamoto et al., 2005).

Statistical analysis

Data are expressed as mean ± sem. Differences between two groups were assessed using the unpaired two-tailed *t*-test and among more than two groups by analysis of variance (ANOVA).

Supplementary Material

Refer to Web version on PubMed Central for supplementary material.

Acknowledgments

We thank the members of the Lewis laboratory for comments and criticism. M. Birnbaum (U. Pennsylvania) is thanked for his gift of the constitutively active AMPK construct. This work was supported by NIH grants to R.E.L (DK52809) and M.H.T. (DK69987, DK59630 and DK56863) and by support from the Nebraska Research Initiative to R.E.L. M.R.F was supported by the Skala Fellowship and M.B. was supported by the Bukey Fellowship from UNMC. K.F. was supported by a Physician/Scientist Training award from the American Diabetes Association. The UNMC Microarray Core Facility receives partial support from NIH grant P20 RR016469. For those studies conducted at USARIEM, the opinions or assertions contained herein are the private views of the author(s) and are not to be construed as official or reflecting the views of the Army or the Department of Defense. Any citations of commercial organizations and trade names in this report do not constitute an official Department of the Army endorsement of approval of the products or services of these organizations.

References

Bergman RN, Kim SP, Catalano KJ, Hsu IR, Chiu JD, Kabir M, Hucking K, Ader M. Why visceral fat is bad: mechanisms of the metabolic syndrome. Obesity (Silver Spring) 2006;14(Suppl 1):16S–19S. [PubMed: 16642958]

Bray GA, York DA. Hypothalamic and genetic obesity in experimental animals: an autonomic and endocrine hypothesis. Physiol Rev 1979;59:719–809. [PubMed: 379887]

Brommage R, Desai U, Revelli JP, Donoviel DB, Fontenot GK, Dacosta CM, Smith DD, Kirkpatrick LL, Coker KJ, Donoviel MS, et al. High-throughput screening of mouse knockout lines identifies true lean and obese phenotypes. Obesity (Silver Spring) 2008;16:2362–2367. [PubMed: 18719666]

Burack WR, Shaw AS. Signal transduction: hanging on a scaffold. Curr Opin Cell Biol 2000;12:211–216. [PubMed: 10712921]

Chaika OV, Chaika N, Volle DJ, Hayashi H, Ebina Y, Wang LM, Pierce JH, Lewis RE. Mutation of tyrosine 960 within the insulin receptor juxtamembrane domain impairs glucose transport but does not inhibit ligand-mediated phosphorylation of insulin receptor substrate-2 in 3T3-L1 adipocytes. J Biol Chem 1999;274:12075–12080. [PubMed: 10207032]

Channavajhala PL, Wu L, Cuozzo JW, Hall JP, Liu W, Lin LL, Zhang Y. Identification of a novel human kinase supporter of Ras (hKSR-2) that functions as a negative regulator of Cot (Tpl2) signaling. J Biol Chem 2003;278:47089–47097. [PubMed: 12975377]

Cunningham JJ. Body composition as a determinant of energy expenditure: a synthetic review and a proposed general prediction equation. Am J Clin Nutr 1991;54:963–969. [PubMed: 1957828]

Dougherty MK, Ritt DA, Zhou M, Specht SI, Monson DM, Veenstra TD, Morrison DK. KSR2 is a calcineurin substrate that promotes ERK cascade activation in response to calcium signals. Mol Cell 2009;34:652–662. [PubMed: 19560418]

Gaidhu MP, Fediuc S, Anthony NM, So M, Mirpourian M, Perry RL, Ceddia RB. Prolonged AICAR-induced AMP-kinase activation promotes energy dissipation in white adipocytes: novel mechanisms integrating HSL and ATGL. J Lipid Res 2009;50:704–715. [PubMed: 19050316]

Hardie DG. AMP-activated/SNF1 protein kinases: conserved guardians of cellular energy. Nat Rev Mol Cell Biol 2007;8:774–785. [PubMed: 17712357]

Harper ME, Green K, Brand MD. The Efficiency of Cellular Energy Transduction and Its Implications for Obesity. Annu Rev Nutr 2008;28:13–33. [PubMed: 18407744]

Kortum RL, Costanzo DL, Haferbier J, Schreiner SJ, Razidlo GL, Wu MH, Volle DJ, Mori T, Sakaue H, Chaika NV, et al. The molecular scaffold kinase suppressor of Ras 1 (KSR1) regulates adipogenesis. Mol Cell Biol 2005;25:7592–7604. [PubMed: 16107706]

Kortum RL, Johnson HJ, Costanzo DL, Volle DJ, Razidlo GL, Fusello AM, Shaw AS, Lewis RE. The molecular scaffold kinase suppressor of Ras 1 is a modifier of RasV12-induced and replicative senescence. Mol Cell Biol 2006;26:2202–2214. [PubMed: 16507997]

Kortum RL, Lewis RE. The molecular scaffold KSR1 regulates the proliferative and oncogenic potential of cells. Mol Cell Biol 2004;24:4407–4416. [PubMed: 15121859]

Kristensen P, Judge ME, Thim L, Ribel U, Christjansen KN, Wulff BS, Clausen JT, Jensen PB, Madsen OD, Vrang N, et al. Hypothalamic CART is a new anorectic peptide regulated by leptin. Nature 1998;393:72–76. [PubMed: 9590691]

Lazar MA. How obesity causes diabetes: not a tall tale. Science 2005;307:373–375. [PubMed: 15662001]

Lowell BB, Spiegelman BM. Towards a molecular understanding of adaptive thermogenesis. Nature 2000;404:652–660. [PubMed: 10766252]

Marsin AS, Bertrand L, Rider MH, Deprez J, Beauloye C, Vincent MF, Van den Berghe G, Carling D, Hue L. Phosphorylation and activation of heart PFK-2 by AMPK has a role in the stimulation of glycolysis during ischaemia. Curr Biol 2000;10:1247–1255. [PubMed: 11069105]

Michaud NR, Therrien M, Cacace A, Edsall LC, Spiegel S, Rubin GM, Morrison DK. KSR stimulates Raf-1 activity in a kinase-independent manner. Proc Natl Acad Sci U S A 1997;94:12792–12796. [PubMed: 9371754]

Mootha VK, Lindgren CM, Eriksson KF, Subramanian A, Sihag S, Lehar J, Puigserver P, Carlsson E, Ridderstrale M, Laurila E, et al. PGC-1alpha-responsive genes involved in oxidative phosphorylation are coordinately downregulated in human diabetes. Nat Genet 2003;34:267–273. [PubMed: 12808457]

Morrison DK, Davis RJ. Regulation of MAP kinase signaling modules by scaffold proteins in mammals. Annu Rev Cell Dev Biol 2003;19:91–118. [PubMed: 14570565]

Mu J, Brozinick JT Jr. Valladares O, Bucan M, Birnbaum MJ. A role for AMP-activated protein kinase in contraction- and hypoxia-regulated glucose transport in skeletal muscle. Mol Cell 2001;7:1085–1094. [PubMed: 11389854]

Muller J, Cacace AM, Lyons WE, McGill CB, Morrison DK. Identification of B-KSR1, a novel brain-specific isoform of KSR1 that functions in neuronal signaling. Mol Cell Biol 2000;20:5529–5539. [PubMed: 10891492]

Muller J, Ory S, Copeland T, Piwnica-Worms H, Morrison DK. C-TAK1 regulates Ras signaling by phosphorylating the MAPK scaffold, KSR1. Mol Cell 2001;8:983–993. [PubMed: 11741534]

Nadler ST, Stoehr JP, Schueler KL, Tanimoto G, Yandell BS, Attie AD. The expression of adipogenic genes is decreased in obesity and diabetes mellitus. Proc Natl Acad Sci U S A 2000;97:11371–11376. [PubMed: 11027337]

Nguyen A, Burack WR, Stock JL, Kortum R, Chaika OV, Afkarian M, Muller WJ, Murphy KM, Morrison DK, Lewis RE, et al. Kinase suppressor of Ras (KSR) is a scaffold which facilitates mitogen-activated protein kinase activation in vivo. Mol Cell Biol 2002;22:3035–3045. [PubMed: 11940661]

Ohmachi M, Rocheleau CE, Church D, Lambie E, Schedl T, Sundaram MV. C. elegans ksr-1 and ksr-2 have both unique and redundant functions and are required for MPK-1 ERK phosphorylation. Curr Biol 2002;12:427–433. [PubMed: 11882296]

Ollmann MM, Wilson BD, Yang YK, Kerns JA, Chen Y, Gantz I, Barsh GS. Antagonism of central melanocortin receptors in vitro and in vivo by agouti-related protein. Science 1997;278:135–138. [PubMed: 9311920]

Ory S, Zhou M, Conrads TP, Veenstra TD, Morrison DK. Protein phosphatase 2A positively regulates Ras signaling by dephosphorylating KSR1 and Raf-1 on critical 14-3-3 binding sites. Curr Biol 2003;13:1356–1364. [PubMed: 12932319]

Pfaffl MW. A new mathematical model for relative quantification in real-time RT-PCR. Nucleic Acids Res 2001;29:e45. [PubMed: 11328886]

Ray P, Monroe FL, Berman JD, Fiedler J. Cyanide sensitive and insensitive bioenergetics in a clonal neuroblastoma x glioma hybrid cell line. Neurochem Res 1991;16:1121–1124. [PubMed: 1795758]

Ritt DA, Zhou M, Conrads TP, Veenstra TD, Copeland TD, Morrison DK. CK2 Is a component of the KSR1 scaffold complex that contributes to Raf kinase activation. Curr Biol 2007;17:179–184. [PubMed: 17174095]

Ruderman NB, Saha AK, Kraegen EW. Minireview: malonyl CoA, AMP-activated protein kinase, and adiposity. Endocrinology 2003;144:5166–5171. [PubMed: 14500570]

Sakamoto K, McCarthy A, Smith D, Green KA, Grahame Hardie D, Ashworth A, Alessi DR. Deficiency of LKB1 in skeletal muscle prevents AMPK activation and glucose uptake during contraction. EMBO J 2005;24:1810–1820. [PubMed: 15889149]

Sanders MJ, Grondin PO, Hegarty BD, Snowden MA, Carling D. Investigating the mechanism for AMP activation of the AMP-activated protein kinase cascade. Biochem J 2007;403:139–148. [PubMed: 17147517]

Schwartz MW, Seeley RJ, Campfield LA, Burn P, Baskin DG. Identification of targets of leptin action in rat hypothalamus. J Clin Invest 1996;98:1101–1106. [PubMed: 8787671]

Shaw RJ, Lamia KA, Vasquez D, Koo SH, Bardeesy N, Depinho RA, Montminy M, Cantley LC. The kinase LKB1 mediates glucose homeostasis in liver and therapeutic effects of metformin. Science 2005;310:1642–1646. [PubMed: 16308421]

Sparti A, DeLany JP, de la Bretonne JA, Sander GE, Bray GA. Relationship between resting metabolic rate and the composition of the fat-free mass. Metabolism 1997;46:1225–1230. [PubMed: 9322812]

Stein SC, Woods A, Jones NA, Davison MD, Carling D. The regulation of AMP-activated protein kinase by phosphorylation. Biochem J 2000;345(Pt 3):437–443. [PubMed: 10642499]

Subramanian A, Tamayo P, Mootha VK, Mukherjee S, Ebert BL, Gillette MA, Paulovich A, Pomeroy SL, Golub TR, Lander ES, et al. Gene set enrichment analysis: a knowledge-based approach for interpreting genome-wide expression profiles. Proc Natl Acad Sci U S A 2005;102:15545–15550. [PubMed: 16199517]

Villena JA, Viollet B, Andreelli F, Kahn A, Vaulont S, Sul HS. Induced adiposity and adipocyte hypertrophy in mice lacking the AMP-activated protein kinase-alpha2 subunit. Diabetes 2004;53:2242–2249. [PubMed: 15331533]

Viollet B, Andreelli F, Jorgensen SB, Perrin C, Geloen A, Flamez D, Mu J, Lenzner C, Baud O, Bennoun M, et al. The AMP-activated protein kinase alpha2 catalytic subunit controls whole-body insulin sensitivity. J Clin Invest 2003;111:91–98. [PubMed: 12511592]

Wu M, Neilson A, Swift AL, Moran R, Tamagnine J, Parslow D, Armistead S, Lemire K, Orrell J, Teich J, et al. Multiparameter metabolic analysis reveals a close link between attenuated mitochondrial

bioenergetic function and enhanced glycolysis dependency in human tumor cells. Am J Physiol Cell Physiol 2007;292:C125–136. [PubMed: 16971499]

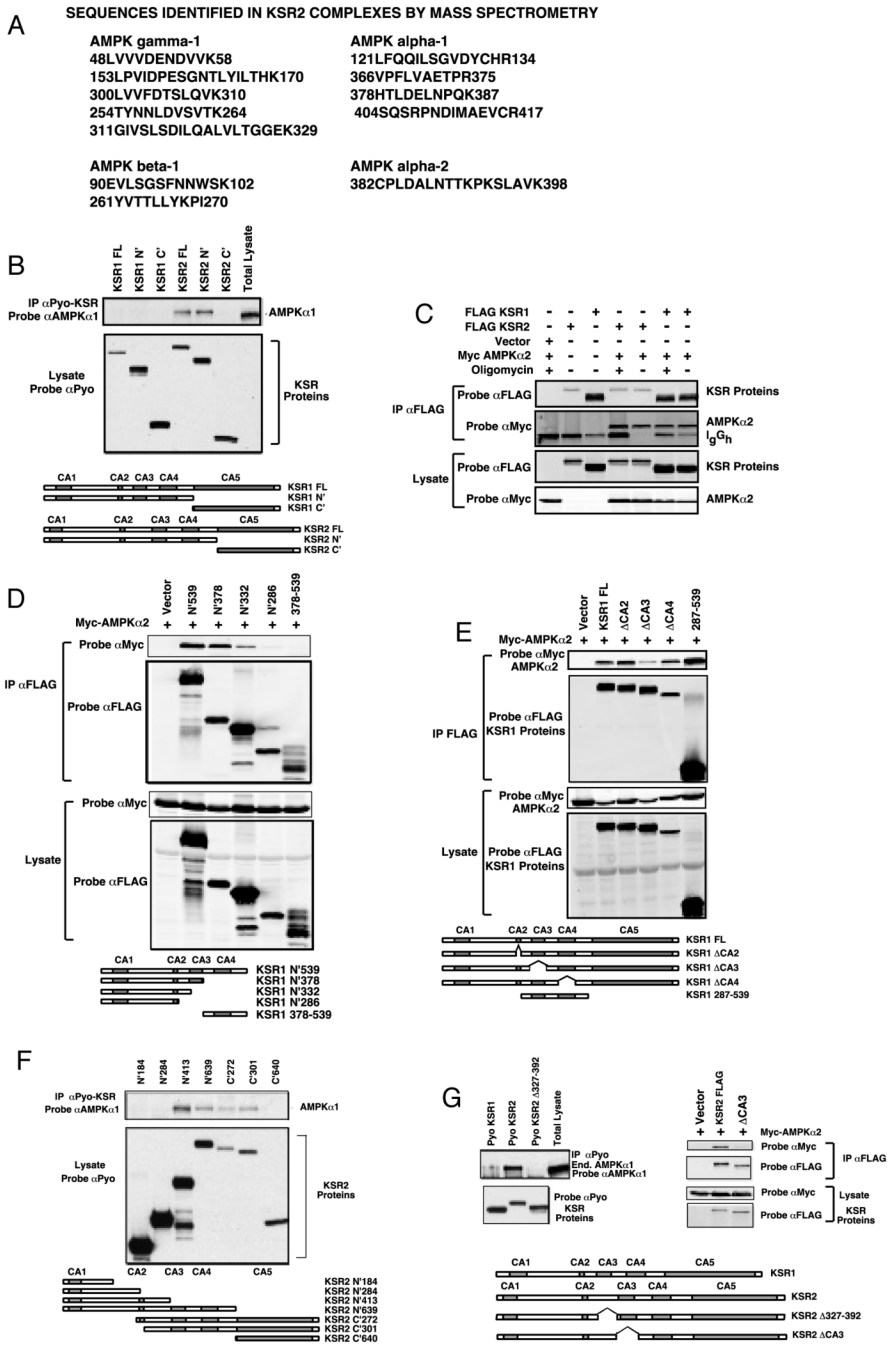

Figure 1. KSR1 and KSR2 interact with AMPK

(A) AMPK-related peptides detected from endogenous proteins co-precipitating with KSR2. KSR2-associated proteins were isolated and peptide fragments were detected by mass spectrometry.

(B) Full length (FL) and truncated Pyo-tagged KSR1 and KSR2 constructs were expressed in COS-7 cells.

(C) FLAG-tagged KSR1 or KSR2 expressed in 293T cells with the Myc-tagged AMPK α subunit. Cells were left untreated or treated with oligomycin.

(D) Truncated FLAG-tagged KSR1 constructs expressed in 293T cells with the Myc-tagged AMPK α subunit.

(E) Deletion constructs of FLAG-tagged KSR1 and the Myc-tagged AMPK α subunit expressed in 293T cells.
(F) Truncated Pyo-tagged KSR2 constructs were expressed in COS-7 cells.
(G) Pyo-tagged full length KSR1, KSR2 or KSR2 with a deletion of amino acids 327-392 expressed in COS-7 cells (left panel). FLAG-tagged full length KSR2 or KSR2 with a deletion of the CA3 region (ΔCA3) expressed with the Myc-tagged AMPK α subunit (right panel).
(B-G) Whole cell lysates and anti-Pyo or anti-FLAG immunoprecipitates were resolved by SDS-PAGE, transferred to nitrocellulose and probed with the indicated antibodies.

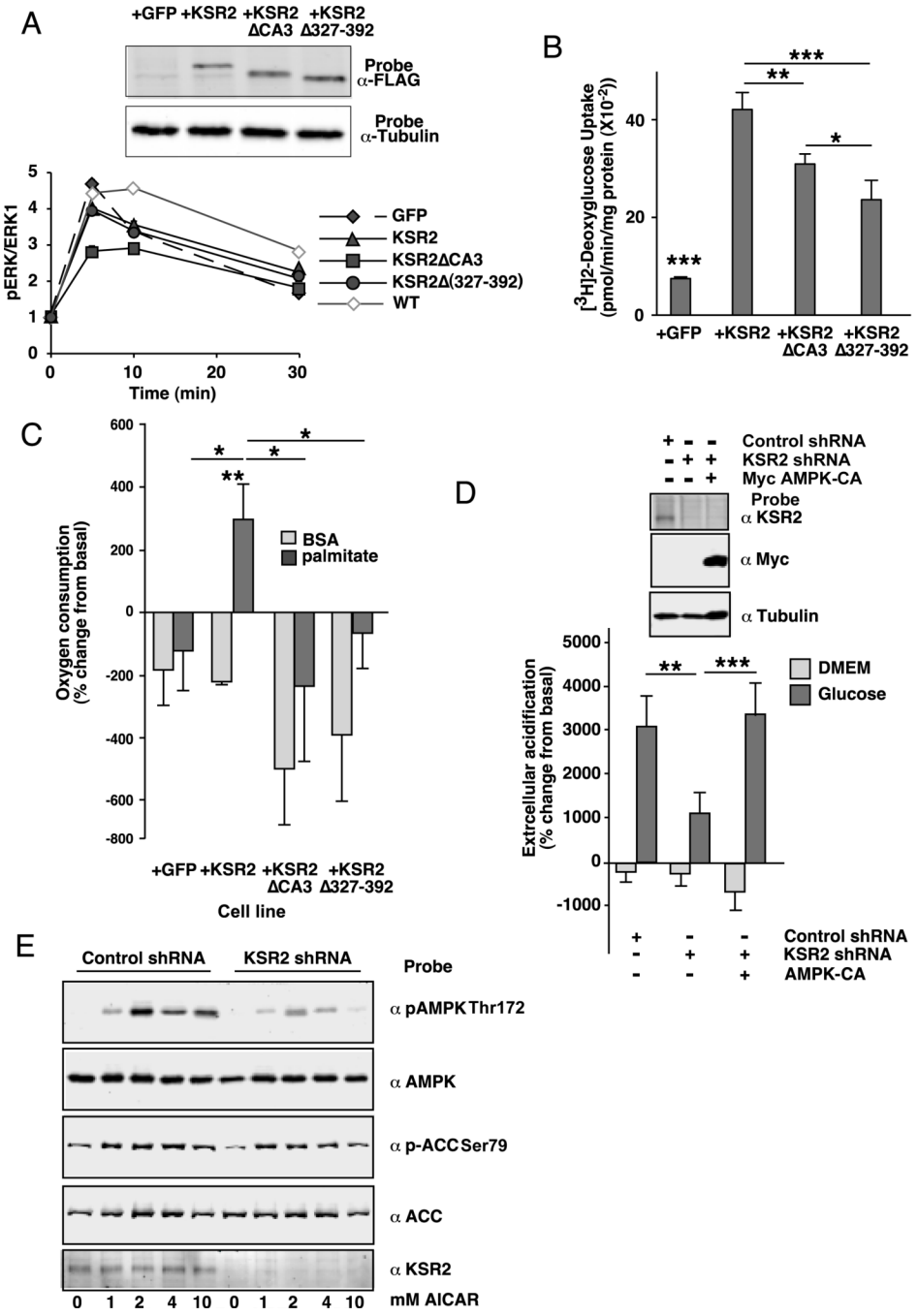

Figure 2. KSR1 expression regulates metabolism in mouse embryo fibroblasts

(A) ERK activation in WT MEFs and *ksr2*$^{-/-}$ MEFs expressing the indicated constructs were treated with 25 ng/ml of PDGF for the indicated times and phosphoERK was detected *in situ*. Representative expression of each construct is shown. Results are the mean ± S.D of triplicate determinations.

(B) Glucose uptake in *ksr2*$^{-/-}$ MEFs and *ksr2*$^{-/-}$ MEFS expressing KSR2, KSR2.ΔCA3, or KSR2.Δ327-392.

(C) FAO in *ksr2*$^{-/-}$ MEFs expressing the indicated constructs.

(D) Glycolysis in NG108-15 cells expressing a non-targeting shRNA, or an shRNA against KSR2 with or without a vector encoding constitutively active AMPK (AMPK-CA). n = 8 for each condition.
(E) NG108-15 cells expressing a non-targeting shRNA, or an shRNA against KSR2 were treated with 0-10 mM AICAR for 30 min at 37°C.
(B-D) *, $P<0.05$; **, $P<0.01$; ***, $P<0.001$.

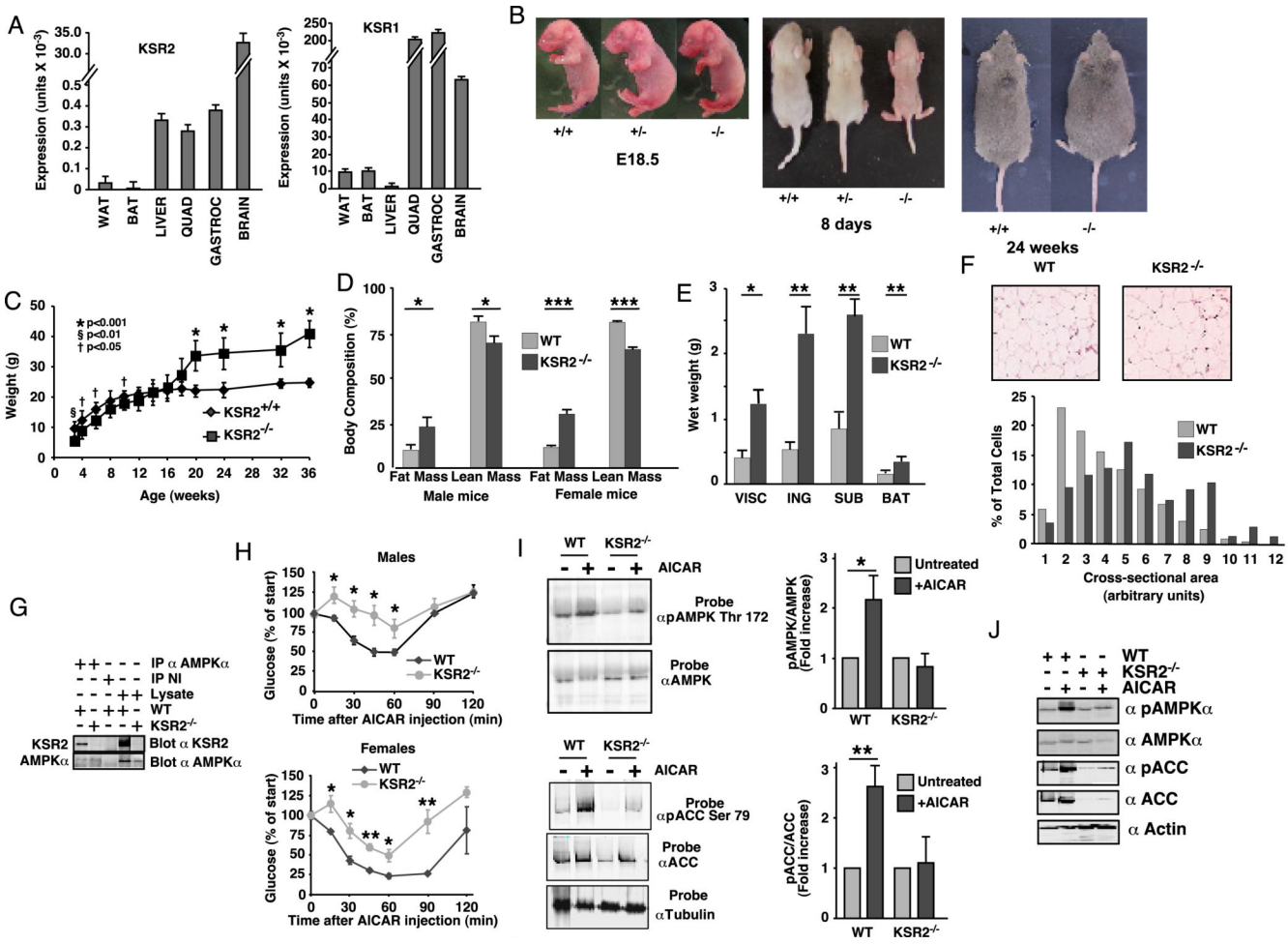

Figure 3. Targeted disruption of *ksr2* causes obesity

(A) Expression of *ksr2* (left panel) and *ksr1* (right panel) mRNA in white adipose tissue (WAT), brown adipose tissue (BAT), liver, quadriceps (QUAD) and gastrocnemius (GASTROC) muscles, and whole brain. The expression of *ksr2* and *ksr1* was normalized relative to the expression of two control genes, *GusB* and *Tbp*, in each tissue.

(B) Null (-/-), heterozygous (+/-) and WT (+/+) mice at day E18.5 (left), eight days (middle) and 24 weeks (right) of age.

(C) Body weights of null (squares, n=8), and WT (diamonds, n=6) mice from three to 36 weeks of age.

(D) Body weight and body composition of 12-week old WT (light bars, n=6 male and 7 female) and *ksr2*$^{-/-}$ (dark bars, n=5 of each sex) mice.

(E) Wet weight of visceral (VISC), inguinal (ING), subcutaneous (SUB) and brown (BAT) adipose depots in WT (light bars, n=4) and *ksr2*$^{-/-}$ mice (dark bars, n=5).

(F) Hematoxylin and eosin staining of histological sections from subcutaneous adipose tissue are shown (upper). Adipocyte cross-sectional area (lower) in WT (light bars) and *ksr2*$^{-/-}$ mice (dark bars).

(G) WT and *ksr2*$^{-/-}$ brain lysates were immunoprecipitated with antibodies to the AMPK α subunit or a non-immune antibody. Immunoprecipitates and representative lysates were probed on western blot for expression of KSR2 and AMPKα.

(H) Blood glucose levels at the indicated times in 6-7 month old WT (circles) and *ksr2*$^{-/-}$ mice (diamonds) following intraperitoneal injection of 0.25 g/kg AICAR. Basal blood glucose levels

(mg/dl) in fed mice were 139.7 ± 8 (KSR2$^{-/-}$ female), 120.7 ± 12 (WT female), 152.8 ± 6 (KSR2$^{-/-}$ male), and 151.8 ± 23 (WT male). n=8 male, 4 female for each genotype.
(I) Western blot analysis of total and phosphoThr172 AMPK α subunit (upper) and total and phosphoSer79 ACC (lower) from white adipose tissue of WT and *ksr2*$^{-/-}$ mice 15 min after injection with 0.25 g/kg AICAR. Graphs show the relative phosphorylation of each protein from five independent experiments.
(J) Phosphorylation of AMPK Thr172 and ACC Ser79 in explants of subcutaneous adipose tissue incubated in DMEM at 37°C for 16 h with and without 1 mM AICAR.
(D, E, H, I) *, $p<0.05$; **, $P<0.01$; ***, $p<0.001$ by single factor ANOVA or (I) unpaired, 2-tailed t-test.

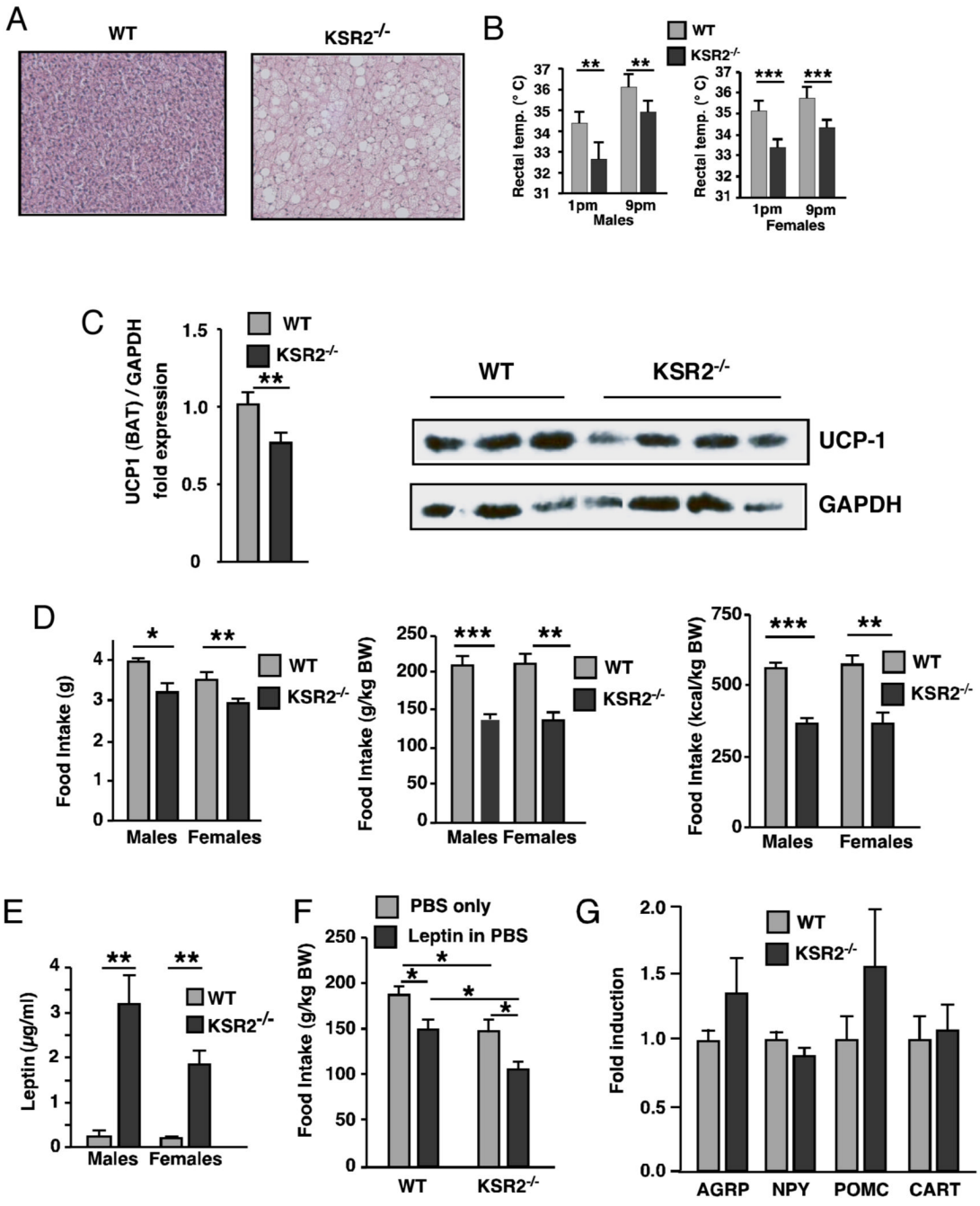

Figure 4. *ksr2*$^{-/-}$ mice are hypothermic and hypophagic

(A) Hematoxylin and eosin staining of brown adipose tissue from WT (left) and *ksr2*$^{-/-}$ (right) mice.

(B) Rectal temperature in 5-6 month old male and female WT (light bars, n=8 for each sex) and *ksr2*$^{-/-}$ mice (dark bars, n=6 males, n=11 females) during light (1 pm) and dark (9 pm) cycles (left panel).

(C) UCP1 mRNA levels in BAT (left panel) in 9-10-month female WT (light bars, n=11) and *ksr2*$^{-/-}$ mice (dark bars, n=5). UCP1 protein levels (right panel) in 8-month WT and *ksr2*$^{-/-}$ female mice.

(D) Average daily food intake in 6 WT males (age 11.5 ± 1.0 weeks), 7 WT females (age 10.6 ± 1.1 weeks), 5 *ksr2*$^{-/-}$ males (age 11.4 ± 0.6 week) and 5 *ksr2*$^{-/-}$ females (age 10.5 ± 1.0 week).
(E) Serum leptin concentrations in 5-6 month WT and *ksr2*$^{-/-}$ mice.
(F) Twenty four hour food intake following control PBS or 5mg/kg leptin injections in WT and *ksr2*$^{-/-}$ mice. n=5 for each genotype.
(G) Neuropeptide mRNA expression in 8-9 month female WT and *ksr2*$^{-/-}$ mice. n=7 for each genotype.
(B, D) *, $P<0.05$; **, $P<0.01$; ***, $P<0.001$

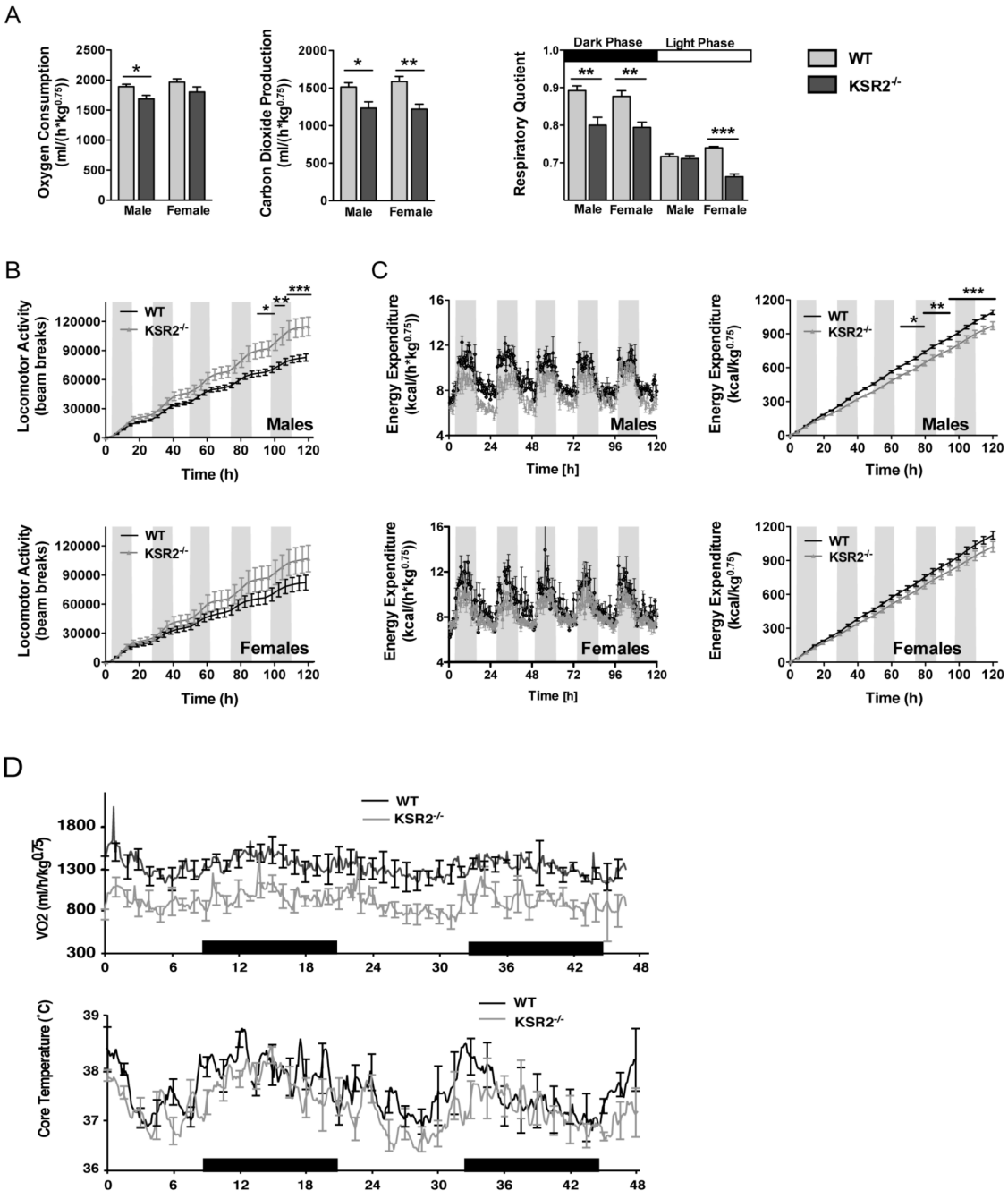

Figure 5. *ksr2*$^{-/-}$ mice are more active, but expend less energy than WT mice

(A) Oxygen consumption (left), carbon dioxide production (middle), and respiratory quotient (right) in WT and *ksr2*$^{-/-}$ mice.

(B) Cumulative locomotor activity in WT and *ksr2*$^{-/-}$ mice.

(C) Spontaneous (middle) and cumulative (right) energy expenditure in male and female WT and *ksr2*$^{-/-}$ mice.

(D) Oxygen consumption (upper panel) and core body temperature of female WT and *ksr2*$^{-/-}$ mice at 32°C.

(A-C) 6 WT males (age 11.5 ± 1.0 weeks), 7 WT females (age 10.6 ± 1.1 weeks), 5 *ksr2*$^{-/-}$ males (age 11.4 ± 0.6 week) and 5 *ksr2*$^{-/-}$ females (age 10.5 ± 1.0 weeks).

(D) 4 WT (age 30.7 ± .02 weeks, and 3 *ksr2*$^{-/-}$ (32.6 ± .07 weeks) female mice.
(A-C) *, P<0.05; **, P<0.01; ***, P<0.001, unpaired, 2-tailed t-test or (C) 2-Way ANOVA with Bonferroni's post hoc test.

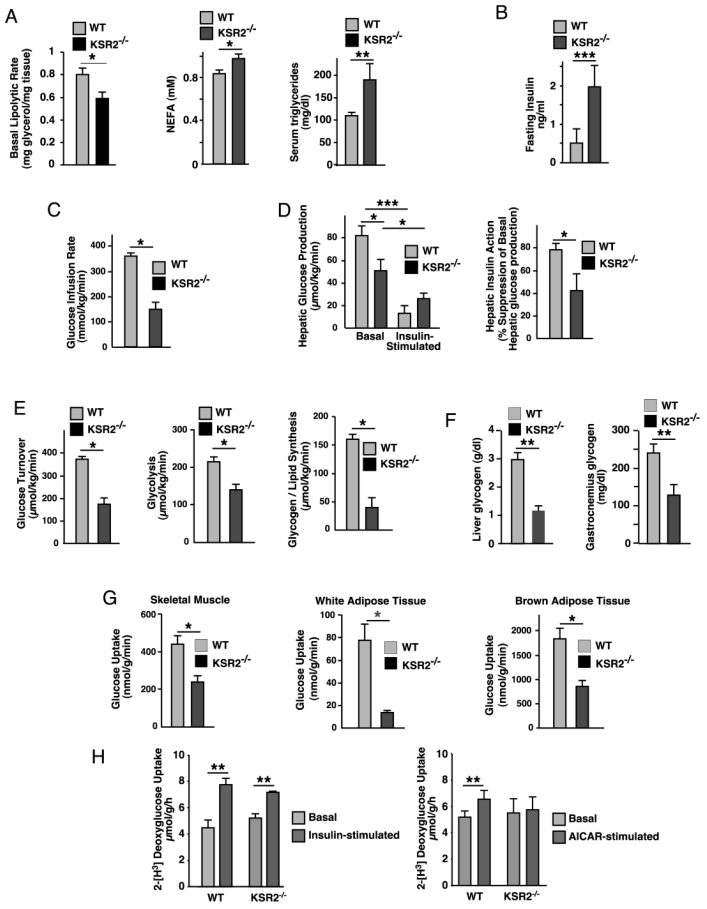

Figure 6. Lipid, glucose and insulin homeostasis is disrupted in *ksr2*$^{-/-}$ mice

(A) Lipolysis (left), serum concentrations of non-esterified free fatty acids (middle) and triglycerides (right) in 5-6 month WT (n=5, left; n=4 middle; n=7, right) and *ksr2*$^{-/-}$ mice (n=6, left; n=3 middle; n=4, right).

(B) Fasting serum insulin in 5-6 month old WT (light bars, n=8) and *ksr2*$^{-/-}$ mice (dark bars, n=8).

(C) Glucose infusion rate, (D) hepatic glucose production and hepatic insulin action, (E) glucose turnover, glycolysis, and glycogen/lipid synthesis in WT (n=11) and *ksr2*$^{-/-}$ mice (n=8).

(F) Tissue glycogen from liver (left) and gastrocnemius (right) in 5-6 month old WT and *ksr2*$^{-/-}$ mice.

(G) Glucose uptake in skeletal muscle, white adipose tissue, and brown adipose tissue, in WT (n=11) and *ksr2*$^{-/-}$ mice (n=8).

(H) *Ex vivo* glucose uptake in isolated EDL muscle from WT and *ksr2*$^{-/-}$ mice treated with 100 nM insulin (left panel, n = 6 WT, 3 *ksr2*$^{-/-}$), or 2 mM AICAR (right panel n = 5 WT, 5 *ksr2*$^{-/-}$).

(A-H) *, P<0.05, **, P<0.01, ***, P<0.001.

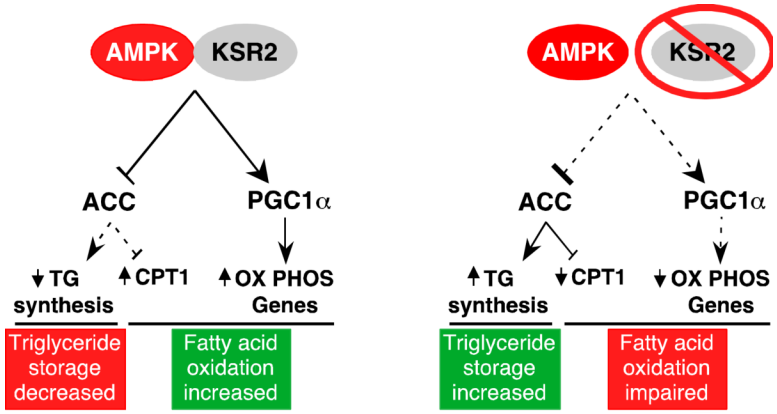

Figure 7. A model of KSR2-mediated regulation of metabolism

Arrows indicate activation. Lines with perpendicular bars attached indicate inhibition. Dashed lines denote decreased function or expression. Arrowheads denote corresponding changes in the amount or activity of the indicated molecule. See text for details.